

# Multidimensional Data Driven Classification of Active Galaxies

Vasileios Stampoulis,<sup>1\*</sup> David A. van Dyk,<sup>1</sup> Vinay L. Kashyap<sup>2</sup> and Andreas Zezas<sup>2,3,4</sup>

<sup>1</sup>Statistics Section, Imperial College London, Huxley Building, South Kensington Campus, London SW7, UK

<sup>2</sup>Harvard-Smithsonian Center for Astrophysics, 60 Garden St., Cambridge, MA 02138, USA

<sup>3</sup>Physics Department, Institute of Theoretical & Computational Physics, University of Crete, Heraklion 71003, Greece

<sup>4</sup>Foundation for Research and Technology-Hellas, Heraklion 71110, Greece

Accepted XXX. Received YYY; in original form ZZZ

## ABSTRACT

We propose a new soft clustering scheme for classifying galaxies in different activity classes using simultaneously 4 emission-line ratios;  $\log([\text{N II}]/\text{H}\alpha)$ ,  $\log([\text{S II}]/\text{H}\alpha)$ ,  $\log([\text{O I}]/\text{H}\alpha)$  and  $\log([\text{O III}]/\text{H}\beta)$ . We fit 20 multivariate Gaussian distributions to spectra obtained from the Sloan Digital Sky Survey (SDSS) in order to capture local structures and subsequently group the multivariate Gaussian distributions to represent the complex multi-dimensional structure of the joint distribution of galaxy spectra in the 4 dimensional line ratio space. The main advantages of this method are the use of all four optical-line ratios simultaneously and the adoption of a clustering scheme. This maximises the available information, avoids contradicting classifications, and treats each class as a distribution resulting in soft classification boundaries. We also introduce linear multi-dimensional decision surfaces using support vector machines based on the classification of our soft clustering scheme. This linear multi-dimensional hard clustering technique shows high classification accuracy with respect to our soft-clustering scheme.

**Key words:** galaxies: active – galaxies: clusters – galaxies: emission lines

## 1 INTRODUCTION

The energy output of galaxies is dominated by two main processes: star-formation and/or accretion onto a supermassive central black-hole, the latter witnessed as an Active Galactic Nucleus (AGN). The interplay between these processes is key for understanding the demographics of galactic activity and the co-evolution of nuclear black-holes and their host galaxies (e.g. Kormendy & Ho 2013). The main tool we have for characterising the type of activity in galaxies is its imprint on the emerging spectrum of the photoionised interstellar medium (ISM). AGN generally produce harder ionising continua which result in stronger high-excitation lines that we can obtain from reprocessing of the spectrum of young stellar populations (e.g. Ferland 2003).

The importance of characterising the ionising source of emission-line regions was recognised early on and led to the first systematic presentation of optical emission-line diagnostic tools by Baldwin, Phillips & Terlevich (1981). This work introduced three diagrams based on four emission-line intensity ratios:  $\log([\text{N II}]/\text{H}\alpha)$ ,  $\log([\text{S II}]/\text{H}\alpha)$ ,  $\log([\text{O I}]/\text{H}\alpha)$  and  $\log([\text{O III}]/\text{H}\beta)$ . These diagrams, known as Baldwin-Phillips-

Terlevich (BPT) diagrams, were able to discriminate between star-forming galaxies (SFGs) and galaxies dominated by AGN activity. At the same time, a third class of galaxies was recognized by Heckman (1980) on the basis of their relatively stronger lower-ionisation lines (Low-Ionisation Nuclear Emission line Regions; LINERs). The format of the BPT diagrams that are typically used today was refined by Veilleux & Osterbrock (1987), and they include all three classes of objects (SFGs, LINERS, AGN).

However, the exact demarcation between SFGs and AGNs is generally defined empirically and hence it is subject to considerable uncertainty. Based on stellar population synthesis and photoionization models Kewley et al. (2001) introduced a maximum ‘starburst’ line on the BPT diagrams which defines the upper bound for the SFGs. Driven by the fact that AGN and SFGs observed in the Sloan Digital Sky Survey (SDSS; York et al. 2000) show two distinct loci extending below the demarcation line of Kewley et al. (2001), a new empirical upper bound for the SFGs was put forward by Kauffmann et al. (2003) in order to distinguish the pure SFGs. The objects between this new empirical SFG line and the demarcation line of Kewley et al. (2001) belong to the class of Composite galaxies (also referred to as Transition objects in previous studies; (e.g. Ho et al. 1997)). The spec-

\* E-mail: vs2712@ic.ac.uk

tra of these Composite galaxies have been traditionally interpreted as the result of significant contributions from both AGN and star-forming activity, although, more recently it has been proposed that their strong high-excitation lines could be the result of shocks (e.g. Rich et al. 2014). Subsequently, Kewley et al. (2006) introduced another empirical line for distinguishing Seyferts and LINERs. More recently, Shi et al. (2015) explored other emission-line intensity ratios that could improve the classification. They used support vector machines to test the classification accuracy using a dataset of galaxies classified as either SFG, AGN, or Composite based on Kauffmann et al. (2003).

The currently used classification scheme suffers from a significant drawback. The use of multiple diagnostic diagrams independently of one another often gives contradicting classifications for the same galaxies (e.g. Ho et al. 1997). According to Kewley et al. (2006), 8% of the galaxies in their sample are characterised as ambiguous in that they were classified as belonging to different classes based on at least two diagnostic diagrams. (For clarity we use the term contradicting to emphasise that the different 2-dimensional diagnostics can give different classifications.) Such contradictions arise because BPT diagrams are projections of a complex multi-dimensional space onto 2-dimensional planes. This limits the power of this diagnostic tool and may lead to inconsistencies between the different diagnostic diagrams. Moreover, the number of extragalactic emission-line objects for which accurate spectra are available has grown rapidly in recent years, especially with the advent of the SDSS. This massive dataset reveals inconsistencies between the theoretical and empirical upper bounds and the actual distribution of the observed line ratios for the different classes (e.g. Kauffmann et al. 2003).

The inefficiency of the existing approach gives rise to the question of whether we can use a multidimensional data-driven method to effectively classify the galaxies. Recently, Vogt et al. (2014), generalised the diagnostics originally proposed by Kewley et al. (2006) by providing multi-dimensional surfaces that separate different activity classes in different groups of diagnostic lines. (These, however, do not include the standard BPT diagnostic ratios).

In this article we propose a classification scheme, the soft allocation data driven (SoDDA) method, which is based on the clustering of galaxy emission-line ratios in the 4-dimensional space defined by the  $[\text{O III}]/\text{H}\beta$ ,  $[\text{N II}]/\text{H}\alpha$ ,  $[\text{S II}]/\text{H}\alpha$ , and  $[\text{O I}]/\text{H}\alpha$  ratios. This is motivated by the clustering of the SFG, AGN, and LINER loci on the 2D projections of the emission-line diagnostic diagrams. Our classification scheme arises from a model that specifies the joint distribution of the emission-line ratios of each galaxy class to be a finite mixture of multivariate Gaussian (MG) distributions. Given the emission line ratios of each galaxy, we compute the posterior probability of each galaxy belonging to each galaxy class. This allows us to achieve a soft clustering. A similar approach was successfully implemented by Mukherjee et al. (1998) in another clustering problem in which they used a mixture of MG distributions to discriminate between distinct classes of gamma-ray bursts.

This paper is organised as follows. In Section 2 we describe the proposed methodology. Section 3 discusses the implementation of the method on galaxy spectra from the SDSS DR8, and Section 4 compares our multidimensional

data driven classification scheme with the one proposed by Kewley et al. (2006). Section 5 introduces multidimensional linear decision boundaries that we compare in terms of their prediction accuracy with both the SoDDA and the scheme of Kewley et al. (2006). In Section 6 we review our results and discuss further research directions.

## 2 CLUSTERING ANALYSIS

Cluster analysis is a statistical method that aims to partition a dataset into subgroups so that the members within each subgroup are more homogeneous (according to some criterion) than the population as a whole. In this article we employ a class of probabilistic (model-based) algorithms that assumes that the data are an identically and independently distributed (i.i.d.) sample from a population described by a density function, which is taken to be a mixture of component density functions. Finite mixture models have been studied extensively as a clustering technique (Wolfe 1970). It is common to assume that the mixture components are all from the same parametric family, such as the Gaussian. The use of mixture models arises naturally in our problem, since the population of galaxies is made up of several homogeneous subgroups: SFGs, Seyferts, LINERs and Composites.

Fraley & Raftery (2002) proposed a general framework to model a population as a mixture of  $K$  subpopulations. Specifically, let  $x_i$  be a vector of length  $p$  containing measurements of object  $i$  ( $i = 1, \dots, n$ ) from a population. In our application the  $x_i$  tabulates the  $p = 4$  emission line ratios for galaxy  $i$ . A finite mixture model expresses the likelihood of  $x_i$  as:

$$p(x_i|\theta, \pi) = \sum_{k=1}^K \pi_k f_k(x_i|\theta_k), \quad (1)$$

where  $f_k$  and  $\theta_k$  are the probability density and parameters for the distribution of subpopulation  $k$ , and  $\pi_k$  is the relative size of subpopulation  $k$ , with  $\pi_k \geq 0$  and  $\sum_{k=1}^K \pi_k = 1$ . Given a sample of  $n$  independent galaxies  $x = (x_1, x_2, \dots, x_n)$ , the joint density can be expressed as:

$$p(x|\theta, \pi) = \prod_{i=1}^n \sum_{k=1}^K \pi_k f_k(x_i|\theta_k), \quad (2)$$

where  $\theta = (\theta_1, \dots, \theta_K)$  and  $\pi = (\pi_1, \dots, \pi_K)$ .

### 2.1 Estimating the parameters of a finite mixture model

Dempster, Laird & Rubin (1977) propose a framework that can be used to compute the maximum likelihood estimators (MLE) in finite mixture models using the Expectation-Maximization (EM) algorithm. Define the unknown parameters as  $\phi = (\theta, \pi)$ . The MLE is  $\phi^* = \text{argmax}_{\phi} p(x|\phi)$ , where  $\text{argmax}_{\phi}$  is an operator that extracts the value of  $\phi$  that maximises the likelihood function,  $p(x|\phi)$ . The EM algorithm is an iterative method for computing the MLE.

In the context of finite mixture models, Dempster et al. (1977) introduced an unobserved vector  $z$  ( $n \times K$ ), where  $z_{i\bullet}$  is the indicator vector of length  $K$  with  $z_{ik} = 1$

if object  $i$  belongs to subpopulation  $k$  and 0 otherwise. Because the  $z_{i\bullet}$  are not observable, they are called latent variables. In this case they specify to which subpopulation each galaxy belongs. Given a statistical model consisting of observed data  $x$ , a set of unobserved latent data  $z$ , and a vector of unknown parameters  $\phi = (\theta, \pi)$ , the EM algorithm iteratively performs alternating expectation (E) and maximisation (M) steps:

E-step: Compute  $Q(\phi|\phi^{(t)}) = E[\log p(x, z|\phi)|x, \phi^{(t)}]$ ,

M-step: Set  $\phi^{(t+1)} = \operatorname{argmax}_{\phi} Q(\phi|\phi^{(t)})$ ,

where the superscript  $t$  indexes the iteration, and  $E[\cdot]$  is the weighted mean evaluated by marginalising over all possible values of  $z$ . The EM algorithm enjoys stable convergence properties, in that the likelihood,  $p(x|\phi)$ , increases in each iteration and the algorithm is known to converge to a stationary point of  $p(x|\phi)$ , which is typically a local maximum.

The joint distribution  $p(x, z|\theta, \pi)$  can be factorised as  $p(x, z|\theta, \pi) = p(z|\theta, \pi)p(x|z, \theta, \pi)$ , where  $p(z|\theta, \pi)$  is a product of  $n$  multinomial distribution  $p(z|\theta, \pi) = \prod_{i=1}^n \prod_{k=1}^K \pi_k^{z_{ik}}$ . Conditional on  $z_{ik} = 1$ ,  $p(x_i) = f_k(x_i|\theta_k)$ . The logarithm of the conditional distribution of  $x$  and  $z$  given  $(\theta, \pi)$ , i.e. the log-likelihood, is:

$$\ell(\theta, \pi|x, z) = \log p(x, z | \theta, \pi) = \sum_{i=1}^n \sum_{k=1}^K z_{ik} \log[\pi_k f_k(x_i|\theta_k)]. \quad (3)$$

The E-step requires us to compute the conditional expectation of Equation 3 given  $(\theta^{(t)}, \pi^{(t)})$ . Because Equation 3 is linear in the components of each  $z_{i\bullet}$ , it suffices to compute the conditional expectation of the components of each  $z_{i\bullet}$  given  $x$  and  $(\theta^{(t)}, \pi^{(t)})$ . This is the conditional probabilities of  $i$  belonging to subpopulation  $k$  given  $(\theta^{(t)}, \pi^{(t)})$ . More specifically:

$$E[z_{ik}|\theta^{(t)}, \pi^{(t)}, x] = \frac{\pi_k^{(t)} f_k(x_i|\theta_k^{(t)})}{\sum_{k=1}^K \pi_k^{(t)} f_k(x_i|\theta_k^{(t)})} = \gamma(z_{ik}) \quad (4)$$

The M-step requires us to maximise the conditional expectation of Equation 3 with respect to  $\pi$  and  $\theta$ , i.e. to maximise  $\sum_{i=1}^n \sum_{k=1}^K \gamma(z_{ik}) \log[\pi_k f_k(x_i|\theta_k)]$ . The particular form of the M-step depends on the choice of density distributions,  $f_k$ , for the subpopulations. Here we assume MG distributions for each subpopulation.

MG mixture models can be used for data with varying structures due to the flexibility in the definition of variance matrices. The density of the MG distribution for subpopulation  $k$  is:

$$f_k(x_i) = \frac{1}{\sqrt{(2\pi)^p |\Sigma_k|}} \exp\left(-\frac{1}{2}(x_i - \mu_k)^T \Sigma_k^{-1} (x_i - \mu_k)\right). \quad (5)$$

The EM formulation for an MG mixture is presented in detail in Dempster et al. (1977). The E-step has the same formulation as in Equation 4, with  $f_k$  given in Equation 5 with  $\theta_k = (\mu_k, \Sigma_k)$ , where  $\mu_k$  represent the means and  $\Sigma_k$  the covariance matrices of the  $x_i$  line ratios for galaxies in subpopulation  $k$ . For the M-step, the updates of the parameters have closed form solutions (Bilmes et al. 1998),

$$\pi_k^{(t+1)} = \frac{1}{n} \sum_{i=1}^n \gamma(z_{ik}) \quad (6)$$

$$\mu_k^{(t+1)} = \frac{\sum_{i=1}^n x_i \gamma(z_{ik})}{\sum_{i=1}^n \gamma(z_{ik})} \quad (7)$$

$$\Sigma_k^{(t+1)} = \frac{\sum_{i=1}^n \gamma(z_{ik})(x_i - \mu_k^{(t+1)})(x_i - \mu_k^{(t+1)})^T}{\sum_{i=1}^n \gamma(z_{ik})}. \quad (8)$$

We implement this EM algorithm using the `scikit-learn` Python library<sup>1</sup> under the constraint that the covariance matrices are full rank, and the diagonal elements cannot be smaller than  $10^{-3}$  to avoid overestimation, i.e. converging to a small number of data points. Because this algorithm can be sensitive to the choice of starting values, we routinely rerun it with 5 different randomly selected sets of starting values. We choose the value among the 5 converged points with the largest likelihood to be the MLE, denoted  $(\pi^*, \mu^*, \Sigma^*)$ .

## 2.2 Choosing the value of $K$

Fraley & Raftery (2002) point out that mixtures of MG distributions are appropriate if the subpopulations are centred at the means,  $\mu_k$ , with increased density for data closer to the means. As a result, the practical use of MG mixture models could be limited if the data exhibit non-Gaussian features, including asymmetry, multi-modality and/or heavy tails. In the SDSS DR8 dataset that we examine, it is apparent that the subpopulations exhibit non Gaussian characteristics such as convexity, skewness and multimodality. In order to account for these non-Gaussian features, we use a mixture of MG distributions with  $K$  considerably larger than the actual number of galaxy classes. In this way, we represent each galaxy class by a mixture of several MG subpopulations. This allows a great deal of flexibility in the class-specific distributions of emission line ratios. With the fitted (large  $K$ ) MG mixture in hand we can then perform hyper-clustering of the  $K$  MG subpopulations so as to concatenate them into clusters representing the four desired galaxy classes.

The number ( $K \gg 4$ ) of MG subpopulations that we fit to our data is chosen using the Bayesian Information Criterion (BIC) of Schwarz et al. (1978) and the gap statistic (Tibshirani et al. 2001). BIC is a model selection criterion based on the maximum log-likelihood obtained with each possible value of  $K$ , and penalised by the increased complexity associated with more subpopulations. More specifically, it is defined as  $\text{BIC}(K) = -2 \cdot L^*(K) + K \log(n)$ , where  $L^*(K) = p(x | \theta^*(K), \pi^*(K))$  is the maximised value of the likelihood when the number of subpopulations is fixed at  $K$ . The value of  $K$  with the lowest BIC is preferred. The gap statistic compares the normalised intra-cluster distances between points in a given cluster,  $W_K$ , for different total number of subpopulations  $K$ , with a null reference distribution obtained assuming data with no obvious clustering. The null reference distribution is generated by sampling uniformly from the original datasets bounding box multiple times. The estimate for the optimal number of subpopulations  $K$  is the

<sup>1</sup> <http://scikit-learn.org/stable/>

value for which the  $W_K$  falls the farthest below the reference curve.

SoDDA accomplishes the hyper-clustering of the  $K$  subpopulations into the four galaxy classes using the classification scheme of [Kewley et al. \(2006\)](#). More specifically, we treat the fitted subpopulations means ( $\mu_1^*, \dots, \mu_K^*$ ) as a dataset and classify them into the four galaxy classes. For example, suppose we fit 10 MG distributions and the means of the distributions 1, 3 and 5 are classified by [Kewley et al. \(2006\)](#) as SFGs, then the distribution of the SFGs under SoDDA would be

$$f_{\text{SFG}}(x_i) = \frac{\pi_1^* f_1(x|\theta_1^*, \pi_1^*) + \pi_3^* f_3(x|\theta_3^*, \pi_3^*) + \pi_5^* f_5(x|\theta_5^*, \pi_5^*)}{\pi_1^* + \pi_3^* + \pi_5^*}. \quad (9)$$

Via the allocations of the means of the  $K$  subpopulations into the four galaxy classes, we have defined the distribution of the emission line ratios for each galaxy class as a finite mixture of MG distributions. Specifically, let  $f_{\text{SFG}}(x)$ ,  $f_{\text{LINER}}(x)$ ,  $f_{\text{Seyfert}}(x)$ , and  $f_{\text{Comp}}(x)$  be the distributions under SoDDA of the emission line ratios of SFGs, LINERs, Seyferts and Composites galaxies respectively. Then, given the four emission line ratios  $x_i$  of a galaxy  $i$ , the posterior probability of galaxy  $i$  belonging to class  $c$  is:

$$\rho_{ic} = \text{Pr}(\text{galaxy } i \text{ is of class } c) \quad (10)$$

$$= \frac{f_c(x)}{\sum_c f_c(x)}, \quad \text{for } c \text{ in } \{\text{SFG, LINER, Seyfert, Comp}\}. \quad (11)$$

### 3 IMPLEMENTATION OF THE CLASSIFICATION SCHEME

The SDSS provides an excellent resource of nuclear spectra of galaxies covering all different activity types (e.g. [Kauffmann et al. 2003](#)). For the definition of our multi-dimensional activity diagnostics we use the ‘‘galspec’’ database of spectral-line measurements from the Max-Planck Institute for Astronomy and Johns Hopkins University group. We used the version of the catalog made publicly available through the SDSS Data Release 8 ([Aihara et al. 2011a,b](#); [Eisenstein et al. 2011](#)), which contains 1,843,200 objects. The spectral-line measurements are based on single Gaussian fits to star-light subtracted spectra, and they are corrected for foreground Galactic absorption ([Tremonti et al. 2004](#); [Kauffmann et al. 2003](#); [Brinchmann et al. 2004](#)). Since the same catalog has been used for the definition of the two-dimensional and multi-dimensional diagnostics of [Kauffmann et al. \(2003\)](#) and [Vogt et al. \(2014\)](#) respectively, it is the best benchmark for testing the SoDDA. From this catalog we selected all objects which have line flux measurements for the 8 diagnostic lines we consider here, with a signal-to-noise ratio (SNR) greater than 6, which ensures the use of reliable line flux measurements for our analysis. The final sample consists of 90,388 galaxies.

We apply the BIC and gap statistic for values of  $K$  ranging from 5 to 50 in increments of 5. Figures 1 and 2 plot the BIC and gap statistics. BIC suggests an optimum value of around  $K = 20$ , while the gap statistic suggests a value of

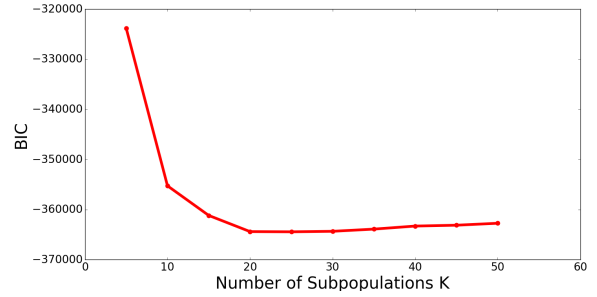


**Figure 1.** The Bayesian Information Criterion (BIC) computed over a grid of values of  $K$  (in increments of 5) using the data of the SDSS DR8. The BIC is a model selection criterion based on the log-likelihood; the model with the lowest BIC value is preferred, indicating that in this case the optimal number of subpopulations is  $K = 20$ .

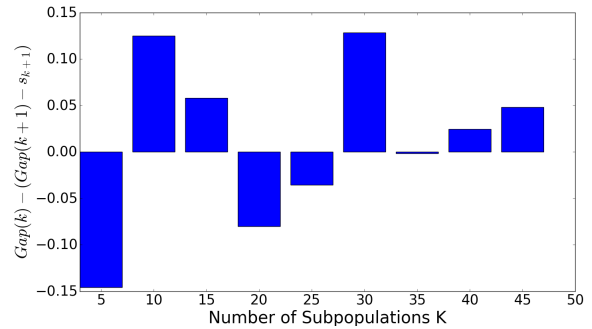


**Figure 2.** The Gap statistic computed over a grid of values of  $K$  (in increments of 5) using the data of the SDSS DR8. The Gap statistic compares the intra-subpopulation distances between points in a given subpopulation with a null reference distribution of the data, i.e., a distribution with no obvious clustering. This figure shows that the smallest value of  $K$  for which the data measure exceeds the randomly generated measure is  $K = 10$ .

$K = 10$ . Since we are ultimately concatenating the subpopulations, we err on the side of large  $K$ , with  $K = 20$ , so as to capture as much detail in the data as possible without overfitting.

Figure 3 displays the BPT diagnostic diagrams for SDSS DR8 with each point colour coded according to its most probable subpopulation among the  $K = 20$  fit. The means of the subpopulations are plotted for  $k = 1, \dots, 20$ . To visualize the spacial extent of each of the 20 subpopulation, Figure 4 plots the  $[\text{N II}]/\text{H}\alpha$  vs  $[\text{O III}]/\text{H}\beta$  diagnostic diagram for each subpopulation. We emphasize that the full 4-dimensional geometry of the subpopulations cannot be seen in the 2-dimensional projections.

Subpopulation 4 is located in a different region in each of the three diagnostic diagrams in Figure 3. Furthermore, the 3-dimensional distribution of Subpopulation 4 is fuzzy, distorted, and totally disjoint from the distribution of the other subpopulations (Figure 5). Inspection of the optical spectra of several of the sources allocated to Subpopulation 4, shows broad emission lines with complex structure. Because these lines cannot be well modelled with the single

**Table 1.** The suggested classification of the 19 subpopulations means.

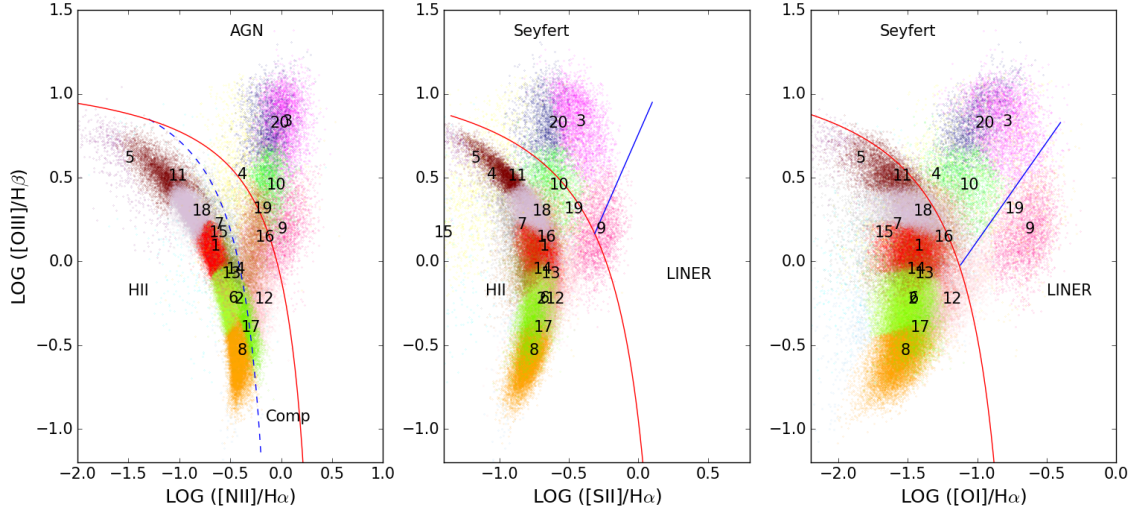
Class	Subpopulation ID
SFG	1,2,5,6,7,8,11,13,14,15,17,18
Seyferts	3,10,20
LINER	9
Composites	12,16,19

Gaussians used, the resulting line measurements are unreliable. Therefore, we discard Subpopulation 4 from our analysis. In order to normalize the probabilities, we divide all the subpopulations weights by  $(1 - \pi_4^*)$ .

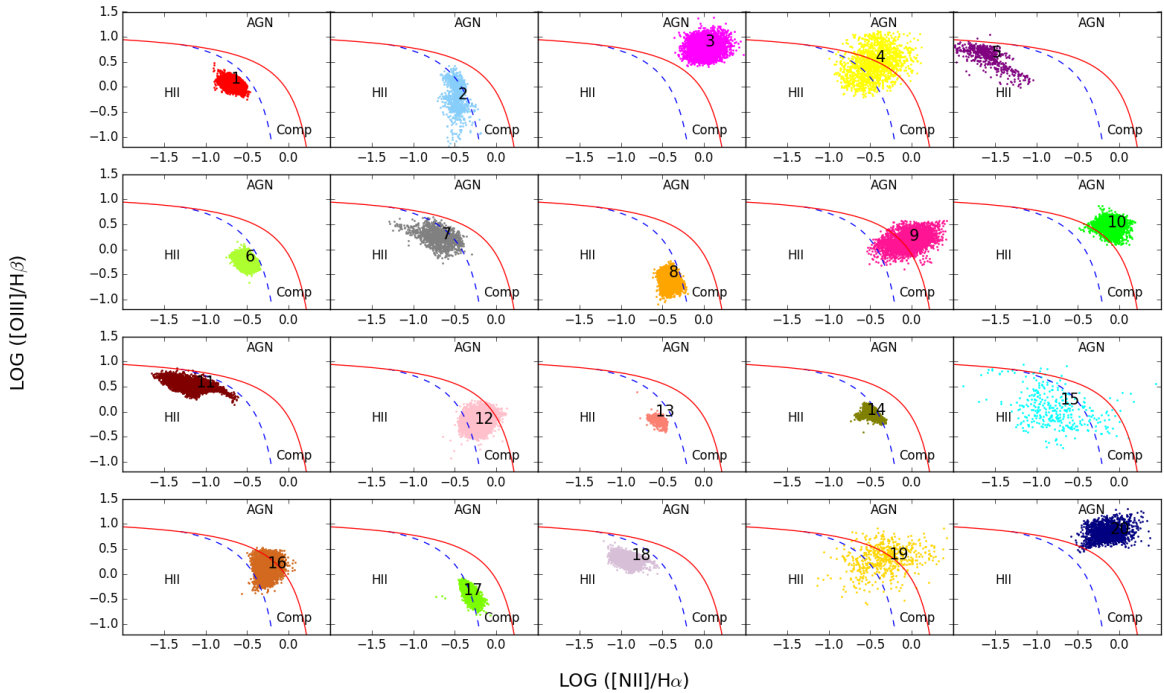
SoDDA associates each of the 19 subpopulations with one activity class based on the projection of their mean on the 2-dimensional BPT diagnostic diagrams, and their location with respect to the activity class separating lines reported in Kewley et al. (2006). The allocations are given in Table 1 for the 19 subpopulations means. Subpopulation 10 transcends the Composite and Seyfert classes. The main discriminator between Composite galaxies and Seyferts is the  $[\text{N II}]/\text{H}\alpha$  diagnostic and the mean of subpopulation 10 is clearly above the maximum ‘starburst’ line on the BPT diagrams introduced by Kewley et al. (2001) as an upper bound of SFGs. Thus, we include Subpopulation 10 in the Seyfert class. After combining the 19 subpopulations to form the 4 galaxy classes as described in Table 1, we compute the posterior probability of each galaxy being a SFG, Seyfert, LINER, or Composite using Equation 11. The second row in Figure 6 shows the BPT diagnostic diagrams for SDSS DR8 with each galaxy colour coded according to its most probable galaxy class (red for SFGs, yellow for Seyferts, blue for LINERs, and green for the Composites) under SoDDA. To highlight the spatial extent of each cluster, we plot the BPT diagrams for each activity class (SFGs, Seyferts, LINERs and Composites) individually in Figure 7.

Figure 8 depicts a 3-dimensional projection of the SDSS DR8 sample on the  $([\text{N II}]/\text{H}\alpha, [\text{S II}]/\text{H}\alpha, [\text{O II}]/\text{H}\beta)$  volume. This 3-dimensional projections illustrate the complex structure of the 4 galaxy activity classes. 3-dimensional rotating projections can be found at <http://hea-www.harvard.edu/AstroStat/etc/gifs.pdf>

SoDDA provides a robust classification for the vast majority of the galaxies in the SDSS DR8 sample. For 90.6% of the galaxies,  $\max_c \rho_{ic}$  is greater than 75%. That is, the most probably class for each of 90.6% of the galaxies has a posterior probability greater than 75%, indicating strong confidence in the adopted classification. Furthermore, the difference between the largest and the second largest  $\rho_{ic}$  (among the classes) is smaller than 1% for only 0.17% of the galaxies, which indicates that the classification is uncertain for very few galaxies. This is illustrated in Figure 9 which plots  $\max_c \rho_{ic}$ , against the difference between  $\max_c \rho_{ic}$  and the second largest  $\rho_{ic}$  among the classes. The red line denotes a difference between the two highest values of  $\rho_{ic}$  (among the classes) of 1%. There are only a few galaxies with a most probably class that is less than 1% (or even 10%) more probably than the second most probably class.



**Figure 3.** The BPT diagnostic diagrams for the SDSS DR8 sample; each galaxy is coloured according to its most probable allocation to one of the 20 subpopulations. The maximum ‘starburst’ line of Kewley et al. (2001) is shown by the solid red line and the empirical upper bound on SFG of Kauffmann et al. (2003) is plotted as dashed blue line. The empirical line for distinguishing Seyferts and LINERs of Kewley et al. (2006) is depicted by the solid blue line.



**Figure 4.** The 20 subpopulations plotted on the  $[NII]/H\alpha$  vs  $[OIII]/H\beta$  projection of the 4-dimensional diagnostic diagram. The subpopulations are numbered following the scheme in Figure 3. This figure shows the spatial extent of each subpopulation and their location with respect to the standard diagnostic lines in the  $[OIII]/H\beta$  diagram. Since these are 2-dimensional projection of the 4-dimensional distribution in each subpopulation, they only give an indication of the extent and location of each subpopulation.

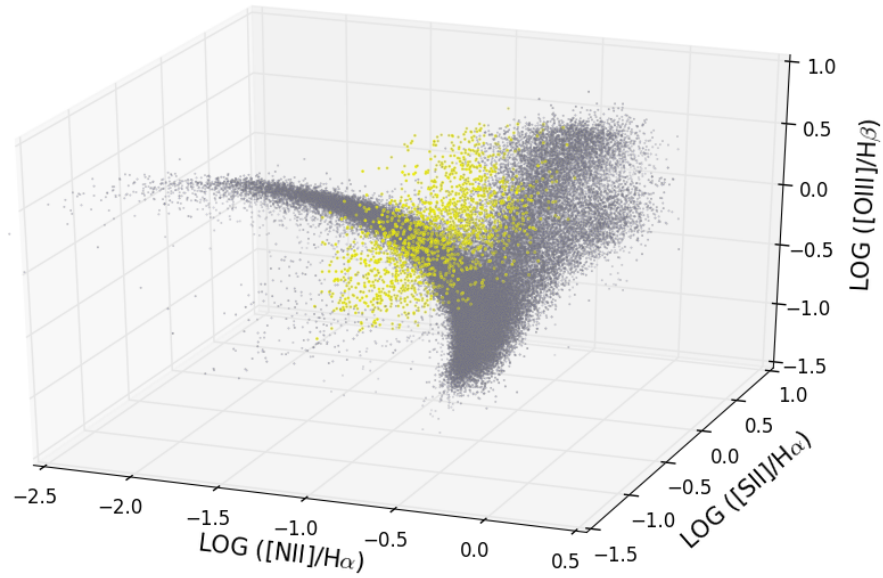


**Figure 5.** A 3-dimensional projection of the SDSS DR8 sample on the  $([\text{N II}]/\text{H}\alpha, [\text{S II}]/\text{H}\alpha, [\text{O III}]/\text{H}\beta)$  volume, showing the locus of the galaxies allocated with Subpopulation 4 (yellow) relative to the other subpopulations (grey). The distribution of Subpopulation 4 is clearly distinct from the that of the other data. The 3-dimensional structure of the joint distribution of the other 19 subpopulations (grey) shows complexities that are lost in its 2-dimensional projections.

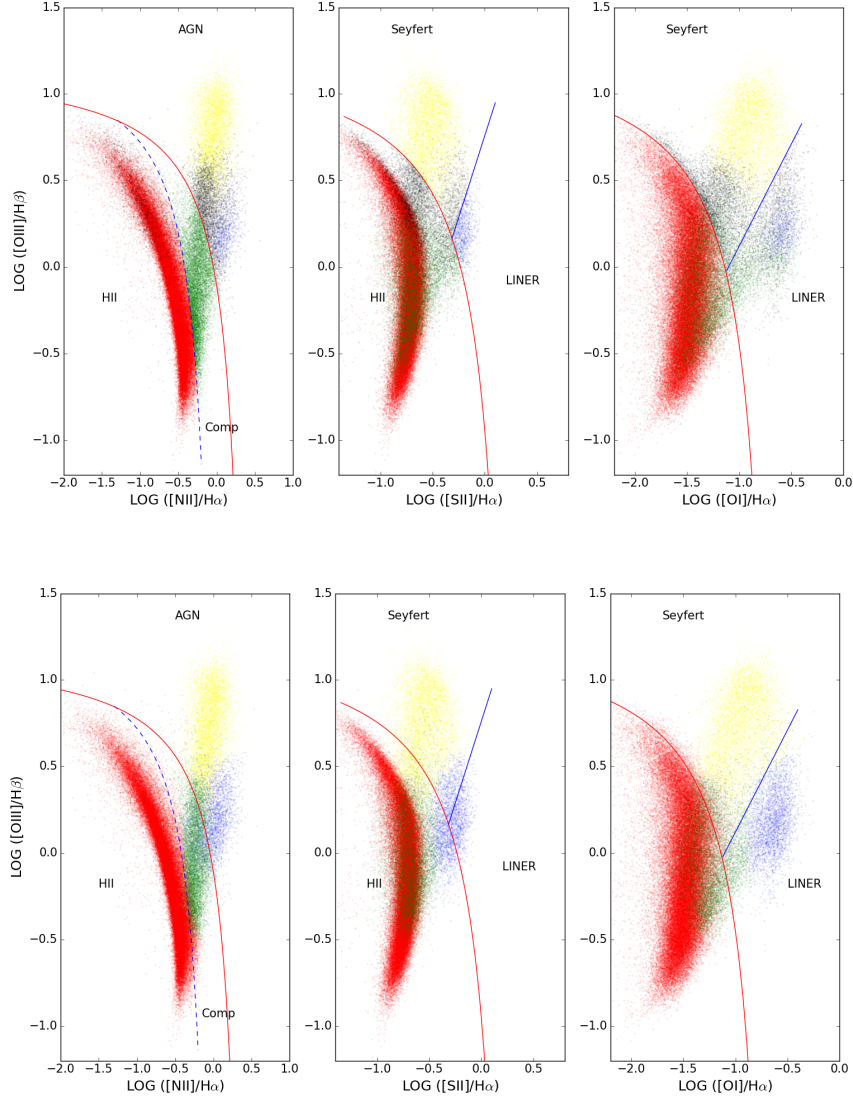


**Figure 6.** The BPT diagrams for the galaxies in the SDSS DR8 sample, based on the Kewley et al. (2006) scheme (top) and SoDDA (bottom). Each galaxy is colour coded according to its classification: red for SFGs, yellow for Seyferts, blue for LINERs, green for the Composite galaxies, and black for the Contradicting classifications. Note the lack of any contradicting classifications (black points) in the SoDDA results (bottom). For reference we also plot the the maximum 'starburst' line of Kewley et al. (2001) (solid red), the empirical upper bound on SFG of Kauffmann et al. (2003) (dashed blue), and the empirical line distinguishing Seyferts and LINERs (Kewley et al. 2006; solid blue). 3-dimensional rotating projections of the 4-dimensional diagram of the SoDDA classification (depicted in the bottom row of the figure in 2-dimensional projections) are available online: <http://hea-www.harvard.edu/AstroStat/etc/gifs.pdf>.



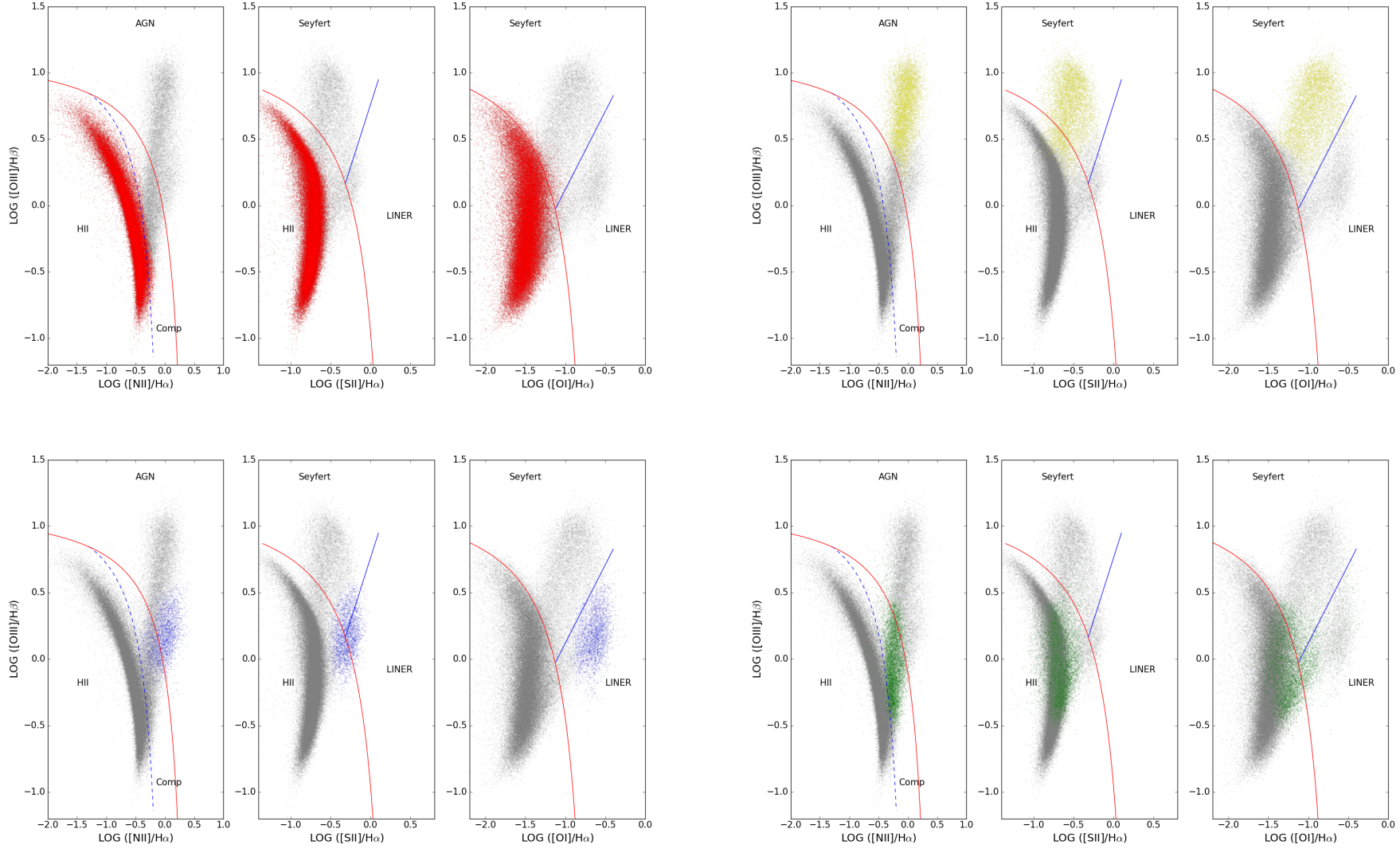


**Figure 7.** The locus of galaxies classified into the different activity types using SoDDA plotted on the three BPT diagrams. Each set of panels shows a different class (clockwise from top left): (a) SFGs (red), (b) Seyfert (yellow); (c) LINERs (blue), (d) Composite (green). For reference the full sample is also plotted in grey. The maximum 'starburst' line of [Kewley et al. \(2001\)](#) is plotted as a solid red line, the empirical upper bound on SFG of [Kauffmann et al. \(2003\)](#) is plotted as a dashed blue line, and the empirical line distinguishing Seyferts and LINERs ([Kewley et al. 2006](#)) is plotted as a solid blue line.

In order to assess the stability of the classification we randomly select a bootstrap sample consisting of 90% of the SDSS DR8 data (sampled without replacement and excluding Subpopulation 4). Using the bootstrap sample, we retune the classifier by estimating the means, weights, and covariance matrices for the 19 subpopulations, assigning each to one of the 4 activity classes, and recalculating the probability that each galaxy (in the SDSS DR8 sample we used for our original analysis excluding Subpopulation 4) belongs to each of the 4 classes. We denote these probabilities,  $\rho_{ic}^{\text{boot}}$ , to distinguish them from those computed with the full SDSS DR8 sample, namely  $\rho_{ic}$ . There is excellent agreement between the original classification and that obtained using the bootstrap sample. Specifically, 99.2% of the galaxies are classified into the same activity type with both classifiers. Similarly, 95.7% of the galaxies classified as Composites using the original classifier are classified in the same way using the set of parameters obtained from using the bootstrap sample. The figures are 96.3% for Seyferts, 97.9% for LINERs, and 99.9% for SFGs.

Overall there is little difference between the class probabilities of the individual galaxies computed with the full data and with the bootstrap sample. To illustrate this, we plot  $\max_c \rho_{ic} - \max_c \rho_{ic}^{\text{boot}}$  against  $\max_c \rho_{ic}$  in Figure 10. Galaxies that are classified differently by the two classifiers are plotted in red. Again, there is excellent agreement: Not only is the classification of the vast majority of galaxies the same for both classifiers, but the probabilities of belonging to the chosen class are both similar and high. Of the few galaxies (0.8%) that are classified differently, 86% have  $\max_c \rho_{ic} < 60\%$ , meaning their classification was not clear to begin with. Overall, our classifier appears robust to the choice of sample used for tuning.

#### 4 COMPARISON WITH 2-DIMENSIONAL CLASSIFICATION SCHEME

In order to show the advantages of our approach, we compare it with the scheme proposed by [Kewley et al. \(2006\)](#). In contrast to the standard approach of using hard thresholds to define the different classes, SoDDA uses soft clustering. We thus calculate the posterior probability of each galaxy belonging to each activity class. Moreover, SoDDA is not based on any particular set of two-dimensional projections of the distributions of emission-line ratios, but rather takes into account the joint distribution of all 4 emission-line ratios. Thus, the main difference between the two schemes is that SoDDA does not produce contradictory classifications for the same galaxy. Rather SoDDA provides a single coherent summary based on *all* diagnostic line ratios: a posterior membership probability for each galaxy.

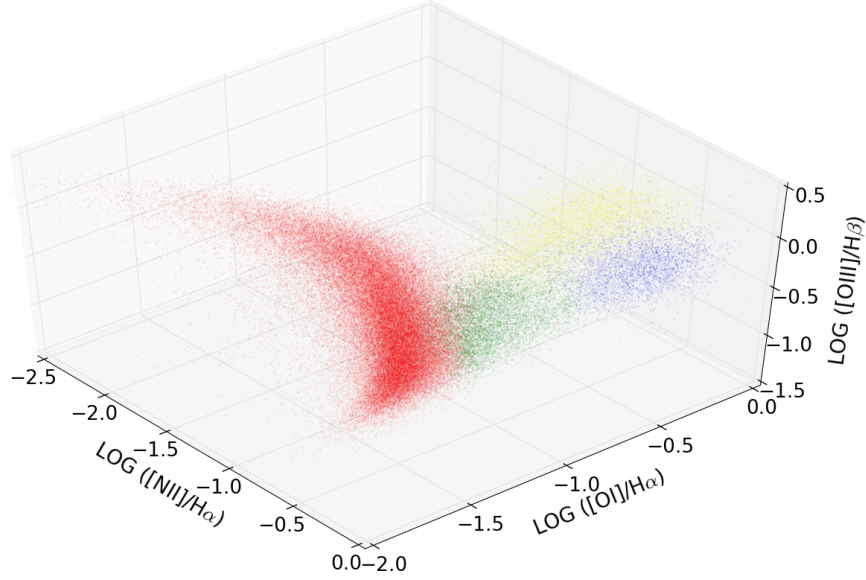


**Figure 8.** A 3-dimensional projection of the SDSS DR8 sample used in our study on the  $([N II]/H\alpha, [S II]/H\alpha, [O III]/H\beta)$  volume, in which each galaxy is colour coded according to its SoDDA classification (red for SFGs, yellow for Seyferts, blue for LINERs and green for the Composites). The 3-dimensional projections illustrates the complex structure of the 4 galaxy activity classes. Each of the four 3-dimensional rotating projection of the full 4-dimensional diagram are available online: <http://hea-www.harvard.edu/AstroStat/etc/gifs.pdf>.

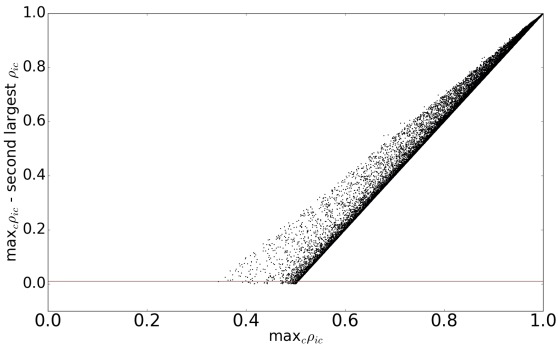


**Figure 9.** The difference between the SoDDA probabilities of the most likely and second most likely class for each galaxy in the SDSS D8 sample. The difference is plotted against the probability of the most likely class. The red line corresponds to a difference of 1%. Only 0.17% of the galaxies exhibit a difference between the probabilities of the most and second most likely classes of less than 1%. 90.6% of the galaxies have  $\max_c \rho_{ic} > 75\%$ , indicating a highly confident classification.

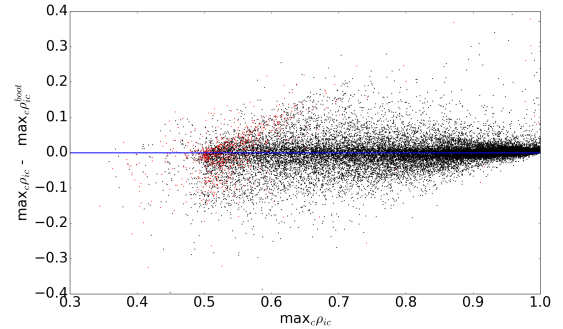


**Figure 10.** A plot of the difference between the class probabilities of the individual galaxies computed with the full data and with the bootstrap sample, namely a plot of  $\max_c \rho_{ic} - \max_c \rho_{ic}^{\text{boot}}$  against  $\max_c \rho_{ic}$ . Galaxies that are classified differently by the two schemes are plotted in red. The vast majority of galaxies have the same classification under both schemes; those that do not (only 0.8% of the full sample) have  $\max_c \rho_{ic} < 60\%$  (86% of them), meaning they lie close to the iso-probability surface between two or more classes.

**Table 2.** A 3-way classification table that compares the SoDDA classification with the standard, 2-dimensional classification scheme (Kewley et al. 2006). Each cell has 3 values: the number of galaxies with (i)  $\rho_{ic} \geq 75\%$ , (ii)  $50\% \leq \rho_{ic} < 75\%$ , and (iii)  $\rho_{ic} < 50\%$ , where  $\rho_{ic}$  is the posterior probability that galaxy  $i$  belongs to galaxy class  $c$  under SoDDA. Contradictory classifications are called ambiguous classifications by Kewley et al. (2006).

SoDDA		Kewley et al. (2006)																	
		SFGs			Seyferts			LINERs			Comp			Contradictory			Total		
	SFGs	65080	946	3	6	0	0	0	0	0	927	1343	69	1744	62	8	67757	2351	80
	Seyferts	0	0	0	5471	262	8	0	0	0	2	28	10	349	1131	45	5822	1421	63
	LINERs	0	0	0	9	33	5	778	4	0	700	181	15	891	234	44	2378	452	64
	Comp	57	251	4	32	40	4	0	0	0	4211	2668	103	258	801	38	4558	3760	149

A 3-way classification table that compares SoDDA with the commonly used scheme proposed by Kewley et al. (2006) appears in Table 2. Each cell has 3 values: the number of galaxies with (i)  $\rho_{ic} \geq 75\%$ , (ii)  $50\% \leq \rho_{ic} < 75\%$ , and (iii)  $\rho_{ic} < 50\%$ , where  $\rho_{ic}$  is the posterior probability that galaxy  $i$  belongs to galaxy class  $c$ . For example, the cell in the first row and first column shows that of the galaxies that both SoDDA and the Kewley et al. (2006) method classify as SFG, 65,080 are SFGs under SoDDA with probability greater than 75%, 946 with probability between 50% and 75%, and only 3 with probability less than 50%. On the other hand, 1,744 of the galaxies that have contradictory classifications according to Kewley et al. (2006) are estimated with SoDDA to be SFGs with probability over 75%, a robust classification.

The first row in Figure 6 shows the classification suggested by Kewley et al. (2006), using the same colour coding as in the second row of Figure 6 (which shows the classification suggested by SoDDA) but with galaxies that are characterised as having contradictory classification plotted in black. The overlap between the composite galaxies (green) and the SFGs (red) is clear in the SoDDA classification (middle and right panels of Figure 6), indicating that the 2-dimensional projection of this 4-dimensional parameter space is insufficient for capturing its complex structure and accurately classifying the galactic activity. The use of hard boundaries defined independently in the 2-dimensional projections is responsible for those galaxies with contradictory classification. On the other hand the probabilistic approach of SoDDA simultaneously accounts for the 4-dimensional structure of the data space and inherently alleviates these inconsistent classifications, while at the same time giving a confident classification of the galaxies to activity classes.

## 5 MULTIDIMENSIONAL DECISION BOUNDARIES

In order to provide a more immediately usable diagnostic in the spirit of the classification lines of Kauffmann et al. (2003) and Kewley et al. (2006), which however, *simultaneously* employ the information in all diagnostic lines, we use a support vector machine (SVM) (Cortes & Vapnik 1995) to obtain multidimensional decision boundaries based on the SoDDA results. A SVM is a discriminative classifier formally defined by a separating hyperplane. In other words, given classified galaxies, the algorithm outputs an optimal hyperplane which can be used to categorize new unlabelled galaxies.

### 5.1 4-dimensional Decision Boundaries

The input data for the derivation of the multidimensional decision boundaries are the 4 emission line ratios for the galaxies in SDSS DR8 sample (i.e.  $x$ ), and the classification for each galaxy as obtained with SoDDA (i.e.,  $y_i$ ). We use the `scikit-learn` Python library to fit the SVM model, employing a linear kernel function. A more complex function did not provide an improvement significant enough to justify its use, especially given the simplicity of a linear kernel. The SVM algorithm requires tuning the cost factor parameter  $C$ , that sets the width of the margin between hyperplanes separating different classes of objects. After a grid search

in a range of values for  $C$ , we suggest a value of  $C = 1$  based on 10-fold cross-validation.  $\mathcal{K}$ -fold cross-validation is a model validation method for estimating the performance of the model. The data is split in  $\mathcal{K}$  roughly equal parts. For each  $\kappa \in (1, \dots, \mathcal{K})$  we fit the model in the other  $\mathcal{K}-1$  parts of the data and calculate the prediction error of the fitted model when predicting the  $\kappa$ th part of the data. By repeating this procedure in a range of values for the model parameters, we choose the values of the parameters that give us the model with the minimum expected prediction error.

Using the SoDDA classification, we employ a SVM approach to define multidimensional surfaces separating the galaxy activity classes. More specifically, we find an optimal separation hyperplane using the 4 emission line ratios for the galaxies from the SDSS DR8 sample and their most probable classification obtained by SoDDA as inputs. The 4-dimensional linear decision boundaries for the four galaxy classes are defined below.

#### SFG:

$$-5.964 \log([\text{N II}]/\text{H}\alpha) - 1.487 \log([\text{S II}]/\text{H}\alpha) - 0.048 \log([\text{O I}]/\text{H}\alpha) - 5.447 \log([\text{O III}]/\text{H}\beta) > 1.562 \quad (12)$$

$$-3.202 \log([\text{N II}]/\text{H}\alpha) - 3.363 \log([\text{S II}]/\text{H}\alpha) - 5.613 \log([\text{O I}]/\text{H}\alpha) + 0.275 \log([\text{O III}]/\text{H}\beta) > 8.072 \quad (13)$$

$$-19.83 \log([\text{N II}]/\text{H}\alpha) - 1.679 \log([\text{S II}]/\text{H}\alpha) - 5.916 \log([\text{O I}]/\text{H}\alpha) - 6.140 \log([\text{O III}]/\text{H}\beta) > 16.98 \quad (14)$$

#### Seyferts:

$$-5.964 \log([\text{N II}]/\text{H}\alpha) - 1.487 \log([\text{S II}]/\text{H}\alpha) - 0.048 \log([\text{O I}]/\text{H}\alpha) - 5.447 \log([\text{O III}]/\text{H}\beta) < 1.562 \quad (15)$$

$$0.42 \log([\text{N II}]/\text{H}\alpha) - 5.391 \log([\text{S II}]/\text{H}\alpha) - 6.899 \log([\text{O I}]/\text{H}\alpha) + 11.90 \log([\text{O III}]/\text{H}\beta) > 11.92 \quad (16)$$

$$6.724 \log([\text{N II}]/\text{H}\alpha) + 4.065 \log([\text{S II}]/\text{H}\alpha) - 2.521 \log([\text{O I}]/\text{H}\alpha) + 10.19 \log([\text{O III}]/\text{H}\beta) > 2.832 \quad (17)$$

#### LINERs:

$$-3.202 \log([\text{N II}]/\text{H}\alpha) - 3.363 \log([\text{S II}]/\text{H}\alpha) - 5.613 \log([\text{O I}]/\text{H}\alpha) + 0.275 \log([\text{O III}]/\text{H}\beta) < 8.072 \quad (18)$$

$$0.420 \log([\text{N II}]/\text{H}\alpha) - 5.391 \log([\text{S II}]/\text{H}\alpha) - 6.899 \log([\text{O I}]/\text{H}\alpha) + 11.90 \log([\text{O III}]/\text{H}\beta) < 11.92 \quad (19)$$

$$2.753 \log([\text{N II}]/\text{H}\alpha) + 11.77 \log([\text{S II}]/\text{H}\alpha) + 5.280 \log([\text{O I}]/\text{H}\alpha) - 1.647 \log([\text{O III}]/\text{H}\beta) > -10.11 \quad (20)$$

#### Composites:

$$-19.83 \log([\text{N II}]/\text{H}\alpha) - 1.679 \log([\text{S II}]/\text{H}\alpha) - 5.916 \log([\text{O I}]/\text{H}\alpha) - 6.140 \log([\text{O III}]/\text{H}\beta) < 16.98 \quad (21)$$

$$6.724 \log([\text{N II}]/\text{H}\alpha) + 4.065 \log([\text{S II}]/\text{H}\alpha) - 2.521 \log([\text{O I}]/\text{H}\alpha) + 10.19 \log([\text{O III}]/\text{H}\beta) < 2.832 \quad (22)$$

$$2.753 \log([\text{N II}]/\text{H}\alpha) + 11.77 \log([\text{S II}]/\text{H}\alpha) + 5.280 \log([\text{O I}]/\text{H}\alpha) - 1.647 \log([\text{O III}]/\text{H}\beta) < -10.11 \quad (23)$$

These multidimensional decision boundaries achieve a mean classification accuracy of about 98% based on 10-fold cross validation with respect to the SoDDA classification. Table 3 compares the SoDDA classification with the proposed classification from the SVM, while Table 4 compares the scheme from Kewley et al. (2006) with the

SVM. We see excellent agreement between the SoDDA and the SVM-based classification. More specifically, 99% of the galaxies classified as SFGs by SoDDA are classified in the same way the SVM-based classification. The figures are 96% for Seyferts, 93% for LINERs, and 88% for Composites. On the other hand, the comparison with the traditional 2-dimensional diagnostics reveals a larger discrepancy owing mainly to the inconsistent classifications between each of the three different diagnostic diagrams.

## 5.2 3-dimensional Decision Boundaries

Because the [O I] line is generally very weak and hence hard to measure, it is common to use the flux ratios of the four other strongest lines in the optical spectrum:  $\log([\text{N II}]/\text{H}\alpha)$ ,  $\log([\text{S II}]/\text{H}\alpha)$ , and  $\log([\text{O III}]/\text{H}\beta)$ , but not for  $\log([\text{O I}]/\text{H}\alpha)$ . Thus, we derive decision boundaries by fitting the SVM algorithm to the SDSS DR8 sample using the SoDDA classification based only on the 3 emission-line ratios ( $\log([\text{N II}]/\text{H}\alpha)$ ,  $\log([\text{S II}]/\text{H}\alpha)$ , and  $\log([\text{O III}]/\text{H}\beta)$ ) as inputs. The resulting 3-dimensional decision surfaces for the four galaxy classes are defined as below.

### SFG:

$$-5.989 \log([\text{N II}]/\text{H}\alpha) - 1.534 \log([\text{S II}]/\text{H}\alpha) - 5.465 \log([\text{O III}]/\text{H}\beta) > 1.543 \quad (24)$$

$$-6.307 \log([\text{N II}]/\text{H}\alpha) - 8.721 \log([\text{S II}]/\text{H}\alpha) - 1.184 \log([\text{O III}]/\text{H}\beta) > 6.781 \quad (25)$$

$$-19.42 \log([\text{N II}]/\text{H}\alpha) - 6.912 \log([\text{S II}]/\text{H}\alpha) - 6.415 \log([\text{O III}]/\text{H}\beta) > 12.62 \quad (26)$$

### Seyferts:

$$-5.989 \log([\text{N II}]/\text{H}\alpha) - 1.534 \log([\text{S II}]/\text{H}\alpha) - 5.465 \log([\text{O III}]/\text{H}\beta) < 1.543 \quad (27)$$

$$0.112 \log([\text{N II}]/\text{H}\alpha) - 10.74 \log([\text{S II}]/\text{H}\alpha) + 10.13 \log([\text{O III}]/\text{H}\beta) > 8.089 \quad (28)$$

$$5.918 \log([\text{N II}]/\text{H}\alpha) + 1.422 \log([\text{S II}]/\text{H}\alpha) + 9.623 \log([\text{O III}]/\text{H}\beta) > 1.611 \quad (29)$$

### LINERs:

$$-6.307 \log([\text{N II}]/\text{H}\alpha) - 8.721 \log([\text{S II}]/\text{H}\alpha) - 1.184 \log([\text{O III}]/\text{H}\beta) < 6.781 \quad (30)$$

$$0.112 \log([\text{N II}]/\text{H}\alpha) - 10.74 \log([\text{S II}]/\text{H}\alpha) + 10.13 \log([\text{O III}]/\text{H}\beta) < 8.089 \quad (31)$$

$$2.383 \log([\text{N II}]/\text{H}\alpha) + 14.56 \log([\text{S II}]/\text{H}\alpha) + 0.378 \log([\text{O III}]/\text{H}\beta) > -6.724 \quad (32)$$

### Composites:

$$-19.42 \log([\text{N II}]/\text{H}\alpha) - 6.912 \log([\text{S II}]/\text{H}\alpha) - 6.415 \log([\text{O III}]/\text{H}\beta) < 12.62 \quad (33)$$

$$5.918 \log([\text{N II}]/\text{H}\alpha) + 1.422 \log([\text{S II}]/\text{H}\alpha) + 9.623 \log([\text{O III}]/\text{H}\beta) < 1.611 \quad (34)$$

$$2.383 \log([\text{N II}]/\text{H}\alpha) + 14.56 \log([\text{S II}]/\text{H}\alpha) + 0.378 \log([\text{O III}]/\text{H}\beta) < -6.724 \quad (35)$$

The multidimensional decision boundaries achieve a mean classification accuracy of about 97% based on 10-fold

cross validation with respect to the SoDDA classification. Table 5 compares the SoDDA classification with the proposed classification from the SVM, while Table 6 compares the scheme from Kewley et al. (2006) with the SVM. As with the 4-dimensional SVM classification, we have excellent agreement with the SoDDA classification and slightly worse agreement with the traditional 2-dimensional diagnostics. Surprisingly, we also find excellent agreement between the 3-dimensional and the 4-dimensional SVM diagnostics indicating that removing the fourth line ratio ( $[\text{O I}]/\text{H}\alpha$ ) does not significantly affect the quality of the classification. More specifically, 99% of the galaxies classified as SFGs by SoDDA are classified in the same way by the 3-dimensional SVM-based classification. The figures are 96% for Seyferts, 89% for LINERs, and 85% for Composites. In other words, removing the ( $[\text{O I}]/\text{H}\alpha$ ) line ratio has no impact on the classification error for SFGs and the Seyferts, and results in a different classification of only 4% of galaxies classified as LINERs by SoDDA and 3% of galaxies classified as Composites by SoDDA, when compared to the complete 4-dimensional diagnostic.

## 6 DISCUSSION

We propose a new soft clustering scheme, the soft allocation data driven (SoDDA) method, for classifying galaxies using emission-line ratios. Our method uses an optimal number of MG subpopulations in order to capture the multi-dimensional structure of the dataset and afterwards concatenate the MG subpopulations into clusters by assigning them to different activity types, based on the location of their means with respect to the loci of the activity classes as defined by Kewley et al. (2006).

The main advantages of this method are the use of all four optical-line ratios simultaneously, thus maximising the available information and avoiding contradicting classifications, and treating each class as a distribution resulting in soft classification boundaries.

An issue with data-driven classification is the question of whether the data have sufficient discriminating power to distinguishing the different activity classes. A strong indication in this direction comes from the fact that the original BPT diagnostic (Baldwin et al. 1981) and its more recent redefinition by Kauffmann et al. (2003) and Kewley et al. (2006) was driven by the clustering of the activity classes in different loci on the 2-dimensional line-ratio diagrams. Furthermore, this distinction was supported by photoionisation models (Kewley et al. 2001, 2013) which indicate that while there is a continuous evolution of the location of sources on the 2-dimensional diagnostic diagrams as a function of their metallicity and hardness of the ionising continuum, star-forming galaxies occupy a distinct region of this diagram. In our analysis we follow a hybrid approach in which we identify clusters based on the multi-dimensional distribution of the object line-ratios, and we associate the clusters with activity types based on their location in the standard 2-dimensional diagnostic diagrams. This gives a physical interpretation to each cluster, while tracing the multi-dimensional distribution of the line ratios.

The fact that our analysis identifies multiple subpopulations within each activity class could indicate that there are

**Table 3.** Comparison of the SoDDA classification with that of the 4-dimensional SVM ( $[\text{O III}]/\text{H}\beta$ ,  $[\text{N II}]/\text{H}\alpha$ ,  $[\text{S II}]/\text{H}\alpha$  and  $[\text{O I}]/\text{H}\alpha$  space).

		SoDDA				
		SFGs	Seyferts	LINERs	Composites	Total
SVM	SFGs	69794	0	0	573	70367
	Seyferts	3	7033	59	273	7368
	LINERs	0	20	2703	143	2866
	Composites	391	253	132	7478	8254
	Total	70188	7306	2894	8467	

**Table 4.** Comparison of the classifications of a 4-dimensional SVM with that of the method by Kewley et al. (2006) ( $[\text{O III}]/\text{H}\beta$ ,  $[\text{N II}]/\text{H}\alpha$ ,  $[\text{S II}]/\text{H}\alpha$  and  $[\text{O I}]/\text{H}\alpha$  space). Contradictory classifications are called ambiguous classifications by Kewley et al. (2006).

		Kewley et al. (2006)					
		SFGs	Seyferts	LINERs	Composites	Contradictory	Total
SVM	SFGs	66199	6	0	2348	1814	70367
	Seyferts	0	5831	0	4	1533	7368
	LINERs	0	22	782	873	1189	2866
	Composites	142	11	0	7032	1069	8254
	Total	66341	5870	782	10257	5605	

**Table 5.** Comparison of the classifications of SoDDA with that of the 3-dimensional SVM ( $[\text{O III}]/\text{H}\beta$ ,  $[\text{N II}]/\text{H}\alpha$ , and  $[\text{S II}]/\text{H}\alpha$  space).

		SoDDA				
		SFGs	Seyferts	LINERs	Composites	Total
SVM	SFGs	69746	0	7	808	70561
	Seyferts	5	7010	99	278	7392
	LINERs	0	66	2574	154	2794
	Composites	437	230	214	7227	8108
	Total	70188	7306	2894	8467	

subclasses that merit special attention. An indication for this is Subpopulation 4. The morphology of this subpopulation is distinct from the others (Figure 5), which can be attributed to the complex spectra of the objects in this cluster.

The approach followed in this paper treats the multi-dimensional emission-line diagnostic diagram as a mixture of different classes. This is a more realistic approach as it does not assume fixed boundaries between the activity classes. Instead, it takes into account the fact that the emission-line ratios of the different activity classes may overlap, which is reflected on the probabilities for an object to belong to a given class. This in fact is reflected in the often inconsistent classification between different 2-dimensional diagnostics (Ho et al. 1997; Yuan et al. 2010), and is clearly seen in the complex structure of the locus of the activity classes in the 3-dimensional rotating diagnostics available in the online supplements. Therefore, the optimal way to characterize a galaxy is by calculating the probability that it belongs to each of the activity classes. This also gives us the possibility to define samples of galaxies in the different classes at various confidence levels.

Another advantage of this approach is that we take into account *all* available information for the activity classification of galactic nuclei. This is important given the complex shape of the multi-dimensional distributions of the emission line ratios (e.g. online 3-dimensional rotating diagnostics; see also Vogt et al. 2014). This way we increase the power of the 2-dimensional diagnostic tools, and eliminate the contradicting classifications they often give. This is demonstrated by the excellent agreement between the classification of the 4-dimensional diagnostic ( $[\text{O III}]/\text{H}\beta$ ,  $[\text{O I}]/\text{H}\alpha$ ,  $[\text{N II}]/\text{H}\alpha$ ,  $[\text{S II}]/\text{H}\alpha$ ) with the 3-dimensional diagnostic excluding the

often weak and hard to detect  $[\text{O I}]$  line ( $[\text{O III}]/\text{H}\beta$ ,  $[\text{O I}]/\text{H}\alpha$ ,  $[\text{N II}]/\text{H}\alpha$ ,  $[\text{S II}]/\text{H}\alpha$ ; see 5.2. This agreement indicates that the loss of the diagnostic power of the  $[\text{O I}]/\text{H}\alpha$  line (which is considered the main discriminator between LINERs and other activity classes (e.g. Kewley et al. 2006) in the 4-dimensional diagnostic, can be compensated by the structure of the locus of the different activity classes which allows their distinction even in the 3-dimensional diagnostic.

Although the probabilistic clustering contains more information about the classification of each active galaxy, the use of hard decision boundaries for classification is effective and closer to the standard approach used in the literature. Therefore, we also present hard classification criteria by employing SVM on the distribution of line-ratios of objects assigned to each activity class. The classification accuracy with these hard criteria is  $\sim 98\%$  when compared to the soft classification (SoDDA). This indicates that the extended tails of the line-ratio distributions of the different activity classes result in only a small degree of overlap and hence misclassification compared to the results we get from SoDDA.

A natural extension of this method is to include additional diagnostic lines (e.g.  $[\text{O II}]$ ), near and far infrared colours (e.g. Stern et al. 2005; Donley et al. 2012), IR line ratios (e.g. PAH,  $[\text{O IV}]$ ,  $[\text{Ne II}]$ ,  $[\text{Ne III}]$ ; e.g. Dale et al. 2006; Tommasin et al. 2010). Such diagnostics have been used extensively in IR surveys in order to address the nature of heavily obscured galaxies, and they are going to be particularly useful for classifying objects detected in JWST surveys. Inclusion of information from other wavebands (e.g. X-ray luminosity, radio luminosity and spectral index, X-ray to optical flux ratio) would further increase the sensitivity of these diagnostic tools by including all available information

**Table 6.** Comparison of the classifications of the 3-dimensional SVM and that of the method by Kewley et al. (2006) ([O III]/H $\beta$ , [N II]/H $\alpha$ , [S II]/H $\alpha$  and [O I]/H $\alpha$  space). Contradictory classifications are called ambiguous classifications by Kewley et al. (2006).

		Kewley et al. (2006)					
		SFGs	Seyferts	LINERs	Composites	Contradictory	Total
SVM	SFGs	66274	5	0	2383	1899	70561
	Seyferts	0	5782	0	5	1605	7392
	LINERs	0	81	782	838	1093	2794
	Composites	67	2	0	7031	1008	8108
	Total	66341	5870	782	10257	5605	

that would allow us to identify obscured and unobscured AGN. Key for these extensions of the diagnostic tools is to incorporate upper-limits (i.e., information about the limiting luminosity in a given band in the case of non detections) and uncertainties in the determination of the clusters in the SoDDA classification or the separating surfaces in the SVM approach.

## ACKNOWLEDGEMENTS

This work was conducted under the auspices of the CHASC International Astrostatistics Center. CHASC is supported by NSF grants DMS 1208791, DMS 1209232, DMS 1513492, DMS 1513484, DMS 1513546, and SI's Competitive Grants Fund 40488100HH0043. We thank CHASC members for many helpful discussions, especially Alexandros Maragkoudakis for providing the data. AZ acknowledges funding from the European Research Council under the European Union's Seventh Framework Programme (FP/2007-2013)/ERC Grant Agreement n. 617001, and support from NASA/ADAP grant NNX12AN05G. This project has been made possible through the ASTROSTAT collaboration, enabled by the Horizon 2020, EU Grant Agreement n. 691164. VLK was supported through NASA Contract NAS8-03060 to the Chandra X-ray Center.

Funding for SDSS-III has been provided by the Alfred P. Sloan Foundation, the Participating Institutions, the National Science Foundation, and the U.S. Department of Energy Office of Science. The SDSS-III web site is <http://www.sdss3.org/>.

SDSS-III is managed by the Astrophysical Research Consortium for the Participating Institutions of the SDSS-III Collaboration including the University of Arizona, the Brazilian Participation Group, Brookhaven National Laboratory, Carnegie Mellon University, University of Florida, the French Participation Group, the German Participation Group, Harvard University, the Instituto de Astrofísica de Canarias, the Michigan State/Notre Dame/JINA Participation Group, Johns Hopkins University, Lawrence Berkeley National Laboratory, Max Planck Institute for Astrophysics, Max Planck Institute for Extraterrestrial Physics, New Mexico State University, New York University, Ohio State University, Pennsylvania State University, University of Portsmouth, Princeton University, the Spanish Participation Group, University of Tokyo, University of Utah, Vanderbilt University, University of Virginia, University of Washington, and Yale University.

## REFERENCES

- Aihara H., et al., 2011a, *ApJS*, **193**, 29  
Aihara H., et al., 2011b, *ApJS*, **195**, 26  
Baldwin J. A., Phillips M. M., Terlevich R., 1981, *PASP*, **93**, 5  
Bilmes J. A., et al., 1998, International Computer Science Institute, 4, 126  
Brinchmann J., Charlot S., White S. D. M., Tremonti C., Kauffmann G., Heckman T., Brinkmann J., 2004, *MNRAS*, **351**, 1151  
Cortes C., Vapnik V., 1995, *Machine learning*, 20, 273  
Dale D. A., et al., 2006, *ApJ*, **646**, 161  
Dempster A. P., Laird N. M., Rubin D. B., 1977, *Journal of the royal statistical society. Series B (methodological)*, pp 1–38  
Donley J. L., et al., 2012, *ApJ*, **748**, 142  
Eisenstein D. J., et al., 2011, *AJ*, **142**, 72  
Ferland G. J., 2003, *ARA&A*, **41**, 517  
Fraleley C., Raftery A. E., 2002, *Journal of the American statistical Association*, 97, 611  
Heckman T. M., 1980, *A&A*, **87**, 152  
Ho L. C., Filippenko A. V., Sargent W. L. W., Peng C. Y., 1997, *ApJS*, **112**, 391  
Kauffmann G., et al., 2003, *MNRAS*, **346**, 1055  
Kewley L. J., Dopita M. A., Sutherland R. S., Heisler C. A., Trevena J., 2001, *ApJ*, **556**, 121  
Kewley L. J., Groves B., Kauffmann G., Heckman T., 2006, *MNRAS*, **372**, 961  
Kewley L. J., Maier C., Yabe K., Ohta K., Akiyama M., Dopita M. A., Yuan T., 2013, *ApJ*, **774**, L10  
Kormendy J., Ho L. C., 2013, *ARA&A*, **51**, 511  
Mukherjee S., Feigelson E. D., Jogesh Babu G., Murtagh F., Fraley C., Raftery A., 1998, *ApJ*, **508**, 314  
Rich J. A., Kewley L. J., Dopita M. A., 2014, *ApJ*, **781**, L12  
Schwarz G., et al., 1978, *The annals of statistics*, 6, 461  
Shi F., Liu Y.-Y., Sun G.-L., Li P.-Y., Lei Y.-M., Wang J., 2015, *Monthly Notices of the Royal Astronomical Society*, 453, 122  
Stern D., et al., 2005, *ApJ*, **631**, 163  
Tibshirani R., Walther G., Hastie T., 2001, *Journal of the Royal Statistical Society: Series B (Statistical Methodology)*, 63, 411  
Tommasin S., Spinoglio L., Malkan M. A., Fazio G., 2010, *ApJ*, **709**, 1257  
Tremonti C. A., et al., 2004, *ApJ*, **613**, 898  
Veilleux S., Osterbrock D. E., 1987, *ApJS*, **63**, 295  
Vogt F. P. A., Dopita M. A., Kewley L. J., Sutherland R. S., Scharwächter J., Basurah H. M., Ali A., Amer M. A., 2014, *ApJ*, **793**, 127  
Wolfe J. H., 1970, *Multivariate Behavioral Research*, 5, 329  
York D. G., et al., 2000, *AJ*, **120**, 1579  
Yuan T.-T., Kewley L. J., Sanders D. B., 2010, *ApJ*, **709**, 884

## APPENDIX A: ONLINE MATERIAL

In the online version of this article, we provide the following:

- (i) Tables in numpy format include the estimated mean  $\mu_k$ , covariance matrix  $\Sigma_k$ , and the weight  $\pi_k$  for each sub-



population  $k = 1, \dots, 20$  (named `means.npy`, `covars.npy`, and `weights.npy` respectively).

(ii) Four text files providing the coefficients and the intercepts for the 4-dimensional and the 3-dimensional surfaces based on the SVM method (Eqs. 12–23, and 24–35 respectively).

(iii) A python script (`classification.py`) that allows the reader to directly apply the SoDDA and the SVM classification. It contains a function that given the 4 emission-line ratios  $\log([\text{N II}]/\text{H}\alpha)$ ,  $\log([\text{S II}]/\text{H}\alpha)$ ,  $\log([\text{O I}]/\text{H}\alpha)$  and  $\log([\text{O III}]/\text{H}\beta)$ , it computes the posterior probability of belonging to each of the 4 activity classes (SFGs, Seyferts, LINERs, and Composites respectively). We also include two functions which give the classification of a galaxy based on the 4-dimensional and the 3-dimensional SVM surfaces given its 4 emission line ratios.

(iv) A file containing sample data that demonstrate the input for the aforementioned functions and scripts.

This paper has been typeset from a  $\text{T}_{\text{E}}\text{X}/\text{L}^{\text{A}}\text{T}_{\text{E}}\text{X}$  file prepared by the author.